Extreme winds and waves in the aftermath of a Neoproterozoic glaciation

Philip A. Allen[1] **& Paul F. Hoffman**[2]

[1]*Department of Earth Sciences, ETH-Zürich, Sonneggstrasse 5, CH-8092 Zürich, Switzerland*
[2]*Department of Earth & Planetary Sciences, Harvard University, 20 Oxford Street, Cambridge, Massachusetts 02138-2902, USA*

The most severe excursions in the Earth's climatic history are thought to be associated with Proterozoic glaciations. According to the 'Snowball Earth' hypothesis, the Marinoan glaciation, which ended about 635 million years ago, involved global or nearly global ice cover. At the termination of this glacial period, rapid melting of continental ice sheets must have caused a large rise in sea level. Here we show that sediments deposited during this sea level rise contain remarkable structures that we interpret as giant wave ripples. These structures occur at homologous stratigraphic levels in Australia, Brazil, Canada, Namibia and Svalbard. Our hydrodynamic analysis of these structures suggests maximum wave periods of 21 to 30 seconds, significantly longer than those typical for today's oceans. The reconstructed wave conditions could only have been generated under sustained high wind velocities exceeding 20 metres per second in fetch-unlimited ocean basins. We propose that these extraordinary wind and wave conditions were characteristic of the climatic transit, and provide observational targets for atmospheric circulation models.

Glacial deposits from the Neoproterozoic era are widespread on virtually every continent, and palaeomagnetic data indicate that ice sheets poured directly into the tropical ocean in at least two discrete glacial episodes—the Sturtian (~710 Myr ago; ref. 1) and the Marinoan (~635 Myr ago; ref. 2)[3]. Globally, both episodes terminated abruptly with the deposition of distinctive carbonate sediments, called cap carbonates, contemporaneous with a major sea level rise[4–7]. Almost all authors of published studies relate the sea level rise to the melting of continental ice sheets, implying a timescale of the order of 2,000 yr (ref. 8) for cap carbonate sedimentation. Sedimentary bedforms consistently observed in cap carbonates contain information concerning wind-generated wave conditions in Neoproterozoic oceans during periods of extreme climatic change.

Marinoan cap carbonates present a panoply of unusual sedimentary structures, which occur in broadly the same stratigraphic order on widely separated palaeocontinental margins (Fig. 1). A continuous basal unit of exceptionally pale-coloured dolostone ($Ca_{0.5}Mg_{0.5}CO_3$), typically 3–20 m thick, is conspicuously laminated. In shelf and upper slope settings, each lamina is defined by a reverse-graded set of peloids (sand-sized pellet-like carbonate aggregates) and a fine micropeloidal drape (Fig. 2d)[5,9]. Some of the larger macropeloids (3 mm in diameter) are broken or faceted[5], and small-scale, low-angle, cross-lamination (Fig. 2d) is ubiquitous. Large microbial bioherms (stromatolites) occur sporadically in the lower part of the dolostone unit; they host peculiar tubular or sheet-like infillings of micropeloidal sediment and/or cement, oriented plumb, the origin of which is controversial[10–13]. Structures interpreted as giant wave ripples, the principal focus of this Article, are concentrated in the upper half of the dolostone unit (Fig. 1). The dolostone unit passes upward, with no significant break in sedimentation, into marly limestone ($CaCO_3$) rhythmites with thin dolostone turbidites. Sea-floor cements (crystal fans) of former aragonite (orthorhombic $CaCO_3$) are variably abundant in the limestone[5,14–18]. The dolostone was clearly deposited within the zone of agitation by storm waves and the limestone in deeper water beyond their reach. The giant wave ripples formed preferentially near the maximum depth of storm wave agitation, where only the longest-period waves feel the sea bed.

Although giant wave ripples are widespread in Marinoan cap dolostones, they are so exceptional relative to common experience that their origin was previously unknown. In the literature, they are described as "tepee" structures[5,15,17], but it has long been recognized that they do not exhibit the planform polygonal pattern and brecciated and contemporaneously cemented crestal zones typical of conventional tepee structures[19], which result from volumetric expansion, like the salt crust of a *playa*. Instead, their crestlines are parallel (Fig. 2b) and oriented sub-normal (40°–90°) to the ancient shelf break. Origination by sliding on the sea floor is inconsistent with their orientation, systematic distribution (Fig. 1) and lack of through-going slip surfaces. Their strongly cylindrical shape (Figs 2b, 3b) is difficult to reconcile with deformation by sediment loading[18]. Where over-steepened flanks of the structures collapsed, leaving truncation surfaces, continued sedimentation re-established the characteristic steep ripple profile. The structures are clearly accretionary and developed *in situ* on the sea bed.

Giant wave ripples are well developed in the northern Canadian Cordillera[5,6,15], where their maximum synoptic relief is typically 20–40 cm and their wavelength 1.5–2.0 m (Table 1). They built up rapidly on the sea bed by aggradation rather than by lateral migration, individual wave ripples maintaining their identity for 1.0–1.5 m vertically (Fig. 3). Individual laminae traverse the chevron-like crestal zone, but they thicken markedly on one flank or the other (Fig. 2a, c, e). The ripple trains develop in a characteristic manner in all areas (Fig. 3b). Initially, the crestlines 'drift' sideways through asymmetric aggradation (Fig. 2e). In the main stage, they aggrade vertically with laminae alternating flank-to-flank (Fig. 2c). At 'senility', the crestlines drift non-uniformly, and are progressively buried by onlapping lamina-sets (Fig. 3b). Crestal angles during the main stage are remarkably small (~110°), and ripple flanks are steep, commonly ranging from 20°–45°, which accounts for the common, localized flank failure. We use only wave ripples unaffected by secondary modification and tectonic deformation in the analysis that follows.

Generation of giant ripples by surface gravity waves

A number of features (Fig. 2) demonstrate that the giant ripples described above were generated by surface gravity waves. These include the near-symmetrical form, trochoidal profile (sharp crests and rounded troughs), bidirectional internal cross-stratification, and chevron-type upbuilding in the crestal region[20]. Collectively, these features indicate an oscillatory flow with flow separation over the bedform crest with each half cycle of the wave motion. However, present-day ripples generated by gravity waves seldom reach more

than a metre in wavelength (λ), and most examples have $\lambda < 20$ cm.

Observations show that bedform steepness (η/λ, where η is bedform height) under oscillatory flows never exceeds 0.20–0.25, a dynamic limit that is below the steepness limited by angle of repose. The dynamic limit in steepness of wave ripples has recently been investigated by evaluating the pressure disturbances generated in the near-bed flow when it undergoes flow separation[21,22]. When flow separation takes place over bedforms, the pressure variations between the crests and troughs of the bedforms dominate, and the effects of sediment concentration appear to be minimal[23], corresponding to the so-called jet regime. In this regime the total friction can be calculated using the friction coefficient $f = 0.36\varepsilon^2$, where $\varepsilon = (\eta/\Lambda_0)^{1/3}$ is a small parameter characterizing the phenomena associated with flow separation, and Λ_0 represents the basic length scale of the flow. The steepness of the giant wave ripples and chevron style upbuilding demonstrate that flow separation took place over their crests. The limiting wave ripple steepness is then given by

$$\left(\frac{\eta}{\lambda}\right)_{\lim} = \beta\frac{f}{\varepsilon} \qquad (1)$$

where β is a constant of the order of one[22]. Substituting for f and ε, and as Λ_0 is equivalent to the amplitude of the wave motion a_0, we obtain:

$$\left(\frac{\eta}{\lambda}\right)_{\lim} = 0.36\beta\left(\frac{\eta}{a_0}\right)^{1/3} \qquad (2)$$

Observations from a wide range of authors on bedform steepness under oscillatory flow demonstrates that equation (2), with $\beta = 1$ and $f = 0.36\varepsilon^2$, is a very good predictor of maximum steepness.

As the wave ripples observed in Marinoan cap carbonates have dimensions far exceeding those compiled from field observations and experiments, a close correspondence between the steepness of the Marinoan structures and the limiting maximum wave ripple steepness given by equation (2) would provide strong independent evidence that the Marinoan wave ripples are indeed bedforms generated under oscillatory flows. Such a correspondence would also give confidence that linear wave theory could be used to reconstruct wind and wave conditions. In the following paragraph, we demonstrate that this is the case.

It is known from a wide range of experimental studies[24] that, for

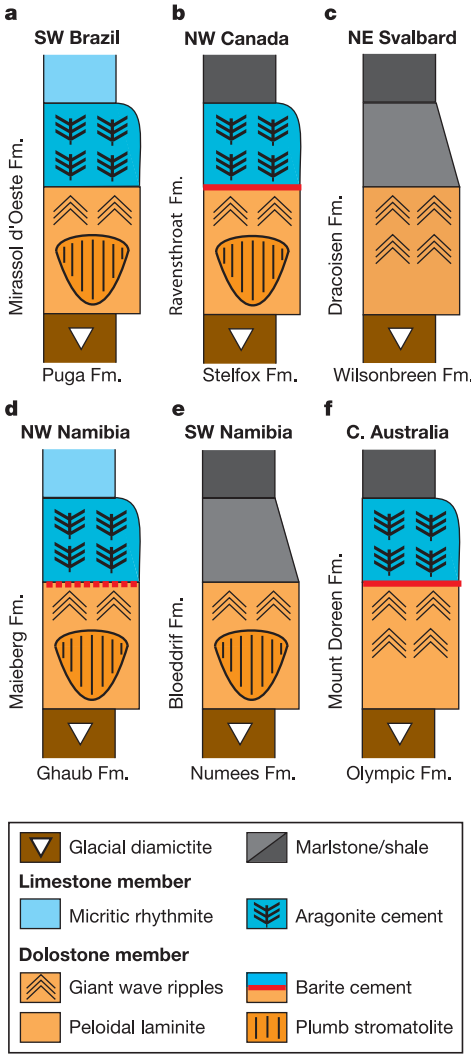

Figure 1 Sequence of sedimentary structures and lithologies in representative Marinoan postglacial cap carbonate sections. Sections are from southwest Brazil[18] (**a**), northwest Canada[5] (**b**), northeast Svalbard[42] (**c**), northwest Namibia[43] (**d**), southwest Namibia[44] (**e**) and central Australia[4] (**f**). Average thickness of the dolostone member in each area is 16 m (**a**), 12 m (**b**), 10 m (**c**), 18 m (**d**), 20 m (**e**) and 4 m (**f**). Giant wave ripples are localized in the upper part of the dolostone member. Fm., formation.

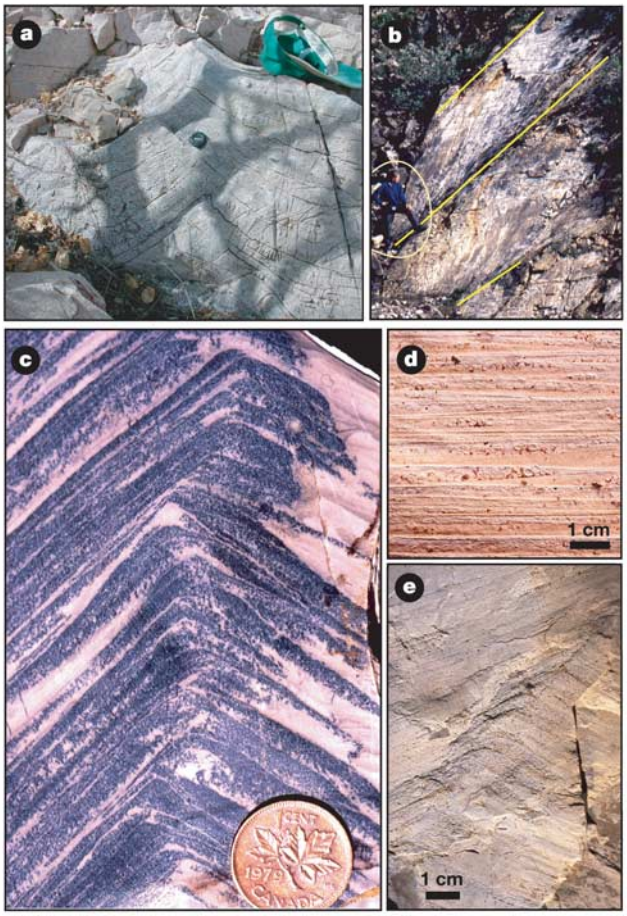

Figure 2 Geometrical features and lamination styles of giant wave ripples in Marinoan post-glacial cap dolostones. **a**, Trochoidal, near-symmetrical wave ripple in cross-section. **b**, Planform view of linear crested wave ripples (yellow lines on crestlines). Circled person for scale. **c**, Crestal zone of aggradational wave ripple, showing chevron-type upbuilding of bidirectional cross-laminae, with thickening of laminae on alternate flanks. The chevron-type upbuilding is a critical observation, demonstrating that the structure grew by alternate deposition on opposing flanks during each half-cycle of the wave motion. **d**, Typical reverse-graded, peloidal dolostone with low-angle cross-lamination. **e**, Aggradational, climbing wave ripple with drift of crestline (to right) typical of early stages of development. Samples from: **a**, northwest Namibia; **b**–**e**, northwest Canada.

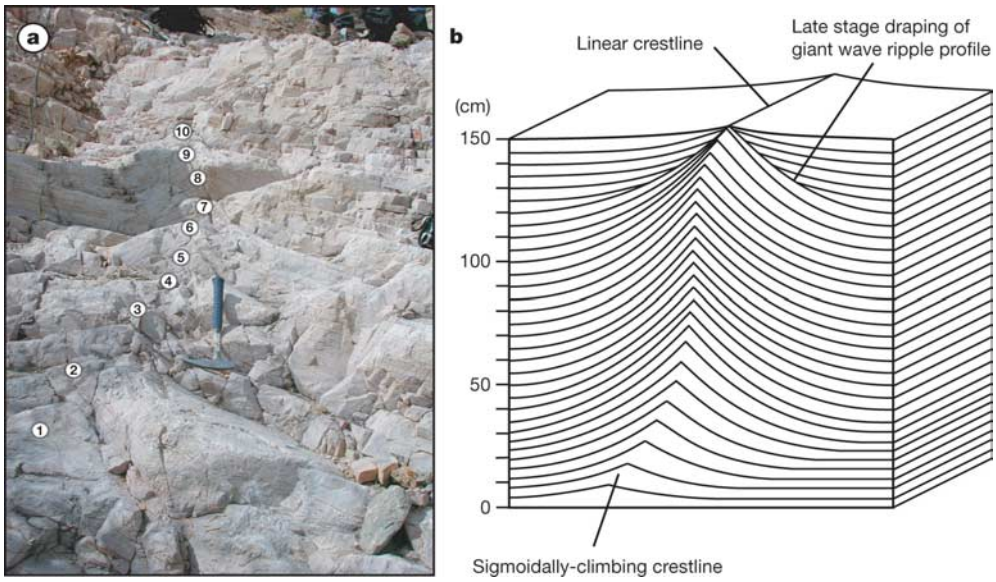

Figure 3 Cross-sectional view of an aggrading (climbing) wave ripple from the Keilberg cap carbonate of the Otavi Platform, northern Namibia. **a**, Sigmoidal drift of crestline position labelled 1 to 10; **b**, generalized line drawing of a Marinoan sigmoidally climbing giant wave ripple. The termination of wave ripple growth is shown by the late-stage laminations that drape and bury the ripple profile.

the steep wave ripples known as 'vortex'[25,26] or 'orbital'[27] types, there is a relationship between wave ripple spacing λ and the amplitude of the near-bed oscillatory flow a_0 given by $\lambda = c2a_0$, where c is a coefficient equal to 0.65 (refs 24, 28). We calculate the amplitude of the near-bed wave motion for the Marinoan wave ripples, and find the theoretical wave ripple steepness on the basis of equation (2). We discover that the Marinoan wave ripples conform very closely to the maximum wave ripple steepness predicted from theory (Table 1). Allowing for the oversimplifications in the analysis, it is beyond reasonable doubt that the Marinoan bedforms are wave-generated vortex ripples, and therefore amenable to analysis of past wave conditions (wave hindcasting)[29–34].

Wave and wind hindcasting

Because the amplitude of wave motion near the bed can be estimated from the steep, near-symmetrical vortex ripples preserved in the Marinoan cap carbonates, linear (Airy) wave theory can be used to calculate the maximum wave period T of formative waves[33,34], as follows. The orbital velocity U_o is calculated for the threshold condition by combining $U_{max} = \pi(2a_0)/T$ and an expression for the threshold velocity under either hydraulically smooth ($D < 0.5$ mm) or rough ($D > 0.5$ mm) flows[35], where D is the mean grain size. The maximum wave period is related to fetch, and therefore gives important palaeogeographical information. Simulation of wave length, wave height and water depth is more problematical, as the amplitude of near-bed motion of water particles is the result of a wave of period T, height H and wavelength L acting in water depth h. Consequently, it is not possible to obtain an unique solution. We simulate gravity waves that transform as they move into shallower water[36,37], and apply two criteria for breaking: a limiting wave steepness in water of finite depth[38] ($(H/L)_{lim} = 0.142\tanh(2\pi h/L)$), and a shallow water breaking criterion[39] ($(H/h)_{lim} = 0.78$). Computer simulations allow the field of formative waves to be established, thereby narrowing down the likely range of palaeowater depth.

The period and height of waves in a fully developed sea are related to the wind speed, wind duration and fetch, but relationships are empirical[40,41]. Taking reconstructed wave periods for the Marinoan giant wave ripples, and assuming a fully developed sea, the most likely wind conditions and wave heights associated with this range of wave period can be estimated.

Hindcasting results

The maximum wave periods calculated for the wave ripples measured in Marinoan cap carbonates are shown in Table 2. The reconstructed maximum wave period is sensitive to the grain size of the sediment, as this strongly affects the threshold velocity under waves. For grain sizes varying between 0.12 and 0.5 mm, and

Table 1 **Measured spacing and height of giant wave ripples**

Location	Spacing (m)	Height (m)	Limiting steepness	Observed steepness
Mackenzie Mountains, Ravensthroat Formation, Windermere Group				
Arctic Red River 64° 55.5′ N, 131° 02′ W	3.5	0.2	0.151	0.057
Arctic Red River	4.0	0.4	0.182	0.100
Arctic Red River	1.5	0.4	0.253	0.267
Cranswick River 65° 05.5′ N, 132° 25′ W	1.5	0.4	0.253	0.267
Svalbard, Lower Dracoisen Formation, Polarisbreen Group				
Nordaustlandet 79° 56.4′ N, 18° 18′ E	5.4	0.38	0.162	0.070
Nordaustlandet	3.0	0.37	0.196	0.123
Nordaustlandet	4.5	0.4	0.175	0.089

Grain size varies from 0.12 to 0.50 mm. Limiting steepness calculated using $\Lambda_0 = a_0$ (ref. 22), determined from $\lambda = (0.65)2a_0$. (Λ_0, length scale of flow; a_0, amplitude of near-bed oscillatory flow; λ, wavelength of ripples.)

Table 2 **Hindcast wave data**

Maximum wave period, T	Wave height, H	Wavelength, L	Water depth, h
30 s*	2.4 m	1,161 m	200 m
30 s*	4.1 m	1,265 m	300 m
30 s*	6.8 m	1,336 m	400 m
30 s*	10.8 m	1,372 m	500 m
30 s*	17.0 m	1,388 m	600 m
21 s†	3.2 m	556 m	100 m
21 s†	7.7 m	657 m	200 m
21 s†	18.3 m	680 m	300 m

Hindcast data were derived from two field localities: Arctic Red River, Mackenzie Mountains, Canada; and Dracoisen Cap, Svalbard. Shown are hindcast maximum wave periods for the Marinoan giant wave ripples, with the wave height and wavelength of formative waves as a function of water depth, calculated using Airy wave theory[33–35].
*Assuming mean grain size $D = 0.12$ mm, deep water wavelength $L_{inf} = 1{,}400$ m.
†Assuming mean grain size $D = 0.5$ mm; deep water wavelength $L_{inf} = 686$ m.

restricting our analysis to the wave ripples close to the limiting bedform steepness[22], maximum wave periods are in the range 21–30 s. This is significantly higher than the typical wave periods in today's oceans.

Wave period in fully developed, fetch-unlimited seas is a function of wind speed. The most likely wind speeds during the Marinoan deglaciation can be estimated by making use of wave energy spectra or co-cumulative power spectra[40]. Within the range of hindcast wave period (21–30 s), co-cumulative power spectra become asymptotic at greater than $\sim$20 m s^{-1}, indicating the upper cut-off for waves contributing to the energy distribution (Fig. 4b). Using energy spectra data, the maximum contribution to the energy spectrum at 20 m s^{-1} wind speed is $T = 14$–20 s (Fig. 4a). Consequently, the Marinoan wave periods can be regarded as exceptional. As wave period is sensitive to fetch, it is clear that the Marinoan wave ripples were produced at the margins of large oceans rather than in restricted settings.

Using the range of wave period above, the water depths at which the giant wave ripples may have formed is extremely wide. However, this large range can be narrowed by considering wave height. The average and 'significant' wave heights in fully developed seas with maximum wave periods in the range 21–30 s, where fetch and wind duration are essentially unlimited, are expected to be >7.5 m and >12 m respectively. Consequently, the water depth range in which the Marinoan wave ripples formed is most likely to be 200–400 m (Table 2).

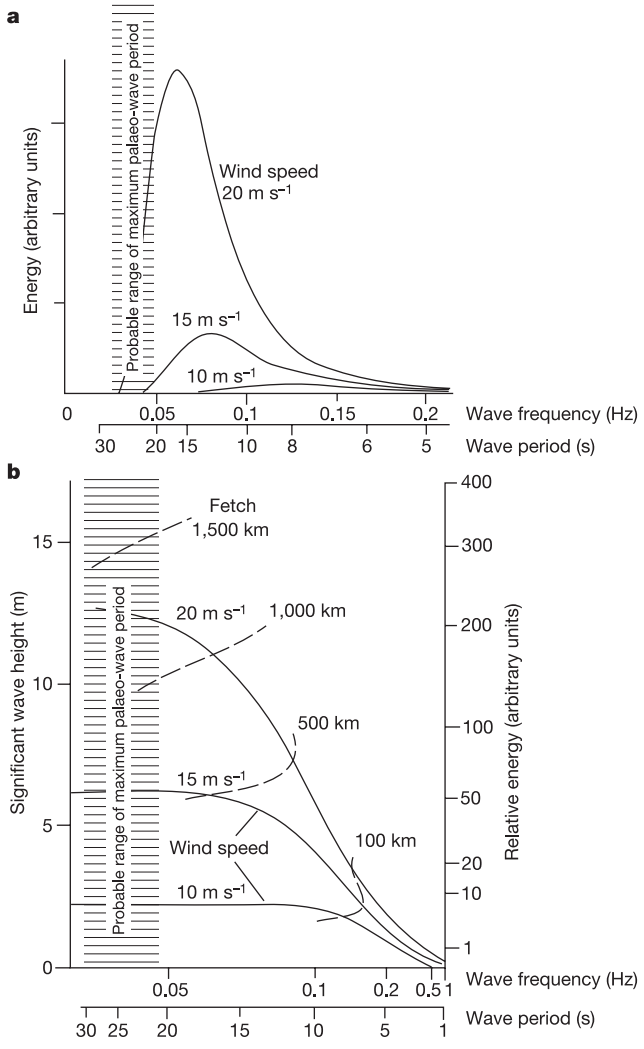

Figure 4 Relation between wind speed, wave period and energy distribution. **a**, Idealized spectra[40] of wave energy versus frequency and period for a fully developed sea for wind speeds of 10–20 m s^{-1}, showing the maximum periods of waves responsible for the formation of giant wave ripples in Marinoan cap carbonates. **b**, Co-cumulative wave spectra[40] for wind speeds of 10–20 m s^{-1}. The slope of the curves indicates the contribution of waves to the energy spectrum. Flat portions of the curves indicate no waves of this period contributing to the energy spectrum.

Implications for climate, oceanography and sedimentology

The occurrence of giant wave ripple marks in Marinoan cap carbonates produced by very long period gravity waves in the Neoproterozoic ocean suggests high horizontal atmospheric pressure gradients during the period of deglaciation. The high-velocity winds and long-period waves of the deglaciation may have had a number of secondary effects. For example, Ekman transports, upwelling, coastal set-up and storm gradient currents should all have been enhanced in the period of deglaciation. In addition, aeolian sediment transport from non-vegetated continental areas should have provided a significant input of dust to the ocean.

The widespread presence and consistent stratigraphic position of giant wave ripples in Marinoan cap carbonates (Fig. 1) suggests that although they represent extreme meteorological conditions, they were typical of the period of deglaciation and represent a palaeogeographically very widespread phenomenon. Furthermore, unlimited fetch and sustained winds are required to produce such long-period waves in the Neoproterozoic oceans. It is unlikely that such conditions could have been produced by short-lived tropical cyclones or hurricanes. We speculate that sustained high-velocity winds developed as a result of the large temperature differences between a shrinking ice cover and a growing low-latitude ocean during the Marinoan deglaciation.

The water depth bracket for the formation of the giant wave ripples (200–400 m) indicates that wave oscillation reached to depths normally associated with quiet, hemipelagic deposition. The absence of giant wave ripples in the immediately overlying stratigraphy suggests that either the exceptional wind conditions ceased as deglaciation proceeded, or that water depths became too great for wave ripples to be formed.

There is a need for atmospheric general circulation modelling to map out boundary conditions under which such unusual wind and wave conditions might prevail, and for geologists to survey the mesoscale and global distribution, orientation and palaeohydrodynamics of these giant wave ripples and the palaeogeography at the time of their formation. □

Received 24 May; accepted 3 November 2004; doi:10.1038/nature03176.

1. Fanning, C. M. & Link, P. U-Pb SHRIMP ages for Neoproterozoic (Sturtian) glaciogenic Pocatello Formation, southeastern Idaho. *Geology* **32,** 881–884 (2004).
2. Hoffmann, K.-H., Condon, D. J., Bowring, S. A. & Crowley, J. L. U-Pb zircon date from the Neoproterozoic Ghaub Formation, Namibia: Constraints on Marinoan glaciation. *Geology* **32,** 817–820 (2004).
3. Evans, D. A. D. Stratigraphic, geochronological, and paleomagnetic constraints upon the Neoproterozoic climatic paradox. *Am. J. Sci.* **300,** 347–433 (2000).
4. Kennedy, M. J. Stratigraphy, sedimentology, and isotope geochemistry of Australian Neoproterozoic postglacial cap dolostones: deglaciation, $\delta^{13}C$ excursions, and carbonate precipitation. *J. Sedim. Res.* **66,** 1050–1064 (1996).
5. James, N. P., Narbonne, G. M. & Kyser, T. K. Late Neoproterozoic cap carbonates, Mackenzie Mountains, northwestern Canada: precipitation and global glacial meltdown. *Can. J. Earth Sci.* **38,** 1229–1262 (2001).
6. Hoffman, P. F. & Schrag, D. P. The snowball Earth hypothesis: testing the limits of global change. *Terra Nova* **14,** 129–155 (2002).
7. Higgins, J. A. & Schrag, D. P. Aftermath of a snowball Earth. *Geochem. Geophys. Geosyst.* **4** (3), 1028, doi:10.1029/2002GC000403 (2003).
8. Hyde, W. T., Crowley, T. J., Baum, S. K. & Peltier, W. R. Neoproterozoic 'snowball Earth' simulations with a coupled climate/ice-sheet model. *Nature* **405,** 425–429 (2000).
9. Xiao, S. *et al.* The Neoproterozoic Quruqtagh Group in eastern Chinese Tianshan: evidence for a post-Marinoan glaciation. *Precambr. Res.* **130,** 1–26 (2004).
10. Cloud, P. E. Jr, Wright, L. A., Williams, E. G., Diehl, P. & Walter, M. R. Giant stromatolites and associated vertical tubes from the Upper Proterozoic Noonday Dolomite, Death Valley region, eastern California. *Geol. Soc. Am. Bull.* **85,** 1869–1882 (1974).
11. Hegenberger, W. Gas escape structures in Precambrian peritidal carbonate rocks. *Commun. Geol. Surv. S.W. Africa/Namibia* **3,** 49–55 (1987).

12. Kennedy, M. J., Christie-Blick, N. & Sohl, L. E. Are Proterozoic cap carbonates and isotopic excursions a record of gas hydrate destabilization following Earth's coldest intervals? *Geology* **29,** 443–446 (2001).
13. Hoffman, P. F., Halverson, G. P. & Grotzinger, J. P. Are Proterozoic cap carbonates and isotopic excursions a record of gas hydrate destabilization following Earth's coldest intervals? Comment and Reply. *Geology* **30,** 286–288 (2002).
14. Peryt, T. M. *et al.* Late Proterozoic aragonitic cement crusts, Bambuí Group, Minas Gerais, Brazil. *Sedimentology* **37,** 279–286 (1990).
15. Aitken, J. D. The Ice Brook Formation and Post-Rapitan, Late Proterozoic glaciation, Mackenzie Mountains, Northwest Territories. *Geol. Surv. Can. Bull.* **404,** 1–43 (1991).
16. Grotzinger, J. P. & Knoll, A. H. Anomalous carbonate precipitates: Is the Precambrian the key to the Permian? *Palaios* **10,** 578–596 (1995).
17. Porter, S. M., Knoll, A. H. & Affaton, P. Chemostratigraphy of Neoproterozoic cap carbonates from the Volta Basin, West Africa. *Precambr. Res.* **130,** 99–112 (2004).
18. Nogueira, A. C. R., Riccomini, C., Sial, A. N., Moura, C. A. V. & Fairchild, T. R. Soft-sediment deformation at the base of the Neoproterozoic Puga cap carbonate (southwestern Amazon craton, Brazil): confirmation of rapid icehouse to greenhouse transition in snowball Earth. *Geology* **31,** 613–616 (2003).
19. Kendall, C. G. St C. & Warren, J. A review of the origin and setting of tepees and their associated fabrics. *Sedimentology* **34,** 1007–1028 (1987).
20. De Raaf, J. F. M., Boersma, J. R. & van Gelder, A. Wave generated structures and sequences from a shallow marine succession, Lower Carboniferous, County Cork, Ireland. *Sedimentology* **4,** 1–52 (1977).
21. Giménez-Curto, L. A. & Corniero, M. A. Flow characteristics in the interfacial shear layer between a fluid and a granular bed. *J. Geophys. Res.* **107** (C5), doi:10.1029/2000JC000729 (2002).
22. Giménez-Curto, L. A. & Corniero, M. A. Highest natural bed forms. *J. Geophys. Res.* **108** (C2), doi:10.1029/2002JC001474 (2003).
23. Giménez-Curto, L. A. & Corniero Lera, M. A. Oscillating turbulent flow over very rough surfaces. *J. Geophys. Res.* **101** (C9), 20745–20758 (1996).
24. Miller, M. C. & Komar, P. D. Oscillation sand ripples generated by laboratory apparatus. *J. Sedim. Petrol.* **50,** 173–182 (1980).
25. Bagnold, R. A. Motion of waves in shallow water. Interactions between waves and sand bottoms. *Proc. R. Soc. Lond. A* **187,** 1–15 (1946).
26. Sleath, J. F. A. On rolling grain ripples. *J. Hydraul. Res.* **14,** 69–80 (1976).
27. Clifton, H. E. in *Beach and Nearshore Sedimentation* (eds Davies, R. A. & Ethington, R. L.) 126–148 (Spec. Publ. 24, Soc. Econ. Mineral. Petrol., Tulsa, Oklahoma, 1976).
28. Miller, M. C. & Komar, P. D. A field investigation of the relationship between oscillation ripple spacing and near-bottom orbital motions. *J. Sedim. Petrol.* **50,** 183–190 (1980).
29. Harms, J. C. Hydraulic significance of some sand ripples. *Geol. Soc. Am. Bull.* **80,** 363–396 (1969).
30. Tanner, W. F. Numerical estimates of ancient waves, water depth and fetch. *Sedimentology* **16,** 71–88 (1971).
31. Komar, P. D. Oscillatory ripple marks and the evaluation of ancient wave conditions and environments. *J. Sedim. Petrol.* **44,** 169–180 (1974).
32. Allen, P. A. Wave-generated structures in the Devonian lacustrine sediments of SE Shetland, and ancient wave conditions. *Sedimentology* **28,** 369–379 (1981).
33. Allen, P. A. Some guidelines in reconstructing ancient sea conditions from wave ripple marks. *Mar. Geol.* **43,** M59–M67 (1981).
34. Allen, P. A. Reconstruction of ancient sea conditions with an example from the Swiss Molasse. *Mar. Geol.* **60,** 455–473 (1984).
35. Komar, P. D. & Miller, M. C. The threshold of sediment motion under oscillatory water waves. *J. Sedim. Petrol.* **43,** 1101–1110 (1973).
36. Wiegel, R. L. *Oceanographical Engineering* (Prentice-Hall, Englewood Cliffs, New Jersey, 1964).
37. Eckart, C. *Gravity Waves* 165–173 (Circular 521, US National Bureau of Standards, 1952).
38. Miche, R. Undulatory movements of the sea in constant and decreasing depth. *Annales Ponts Chaussée* May-June, July-August, 25–78, 131–164, 270–292, 369–406 (1944).
39. McCowan, J. On the highest wave of permanent type. *Phil. Mag.* **5,** 351–357 (1894).
40. Pierson, W. J., Neumann, G. & James, R. W. *Practical Methods for Observing and Forecasting Ocean Waves* (Publ. 603, US Naval Oceanographic Office, Washington DC, 1955).
41. Coastal Engineering Research Center. *Shore Protection Manual* Vols 1–3 (US Army Corps of Engineers, Washington DC, 1973).
42. Halverson, G. P., Maloof, A. C. & Hoffman, P. F. The Marinoan glaciation (Neoproterozoic) in northeast Svalbard. *Basin Res.* **16,** 297–324 (2004).
43. Hoffman, P. F. Carbonates bounding glacial deposits: Evidence for Snowball Earth episodes and greenhouse aftermaths in the Neoproterozoic Otavi Group of northern Namibia. In *Excursion Guide, 16th Int. Sedimentological Conf.* (International Association of Sedimentologists, 2002).
44. Fölling, P. G. & Frimmel, H. E. Chemostratigraphic correlation of carbonate successions in the Gariep and Saldania Belts, Namibia and South Africa. *Basin Res.* **14,** 69–88 (2002).

Acknowledgements P.F.H. thanks the Arctic Natural Science and Earth System History Programs (NSF), the Astrobiology Institute (NASA) and the Earth System Evolution Program (CIAR) for supporting this work. We thank A. Bush, H. Daigle, C. Ferguson, W. Fischer, P. Halverson, A. Maloof, P. Myrow and S. Turchyn for discussions.

Competing interests statement The authors declare that they have no competing financial interests.

Correspondence and requests for materials should be addressed to P.A.A. (philip.allen@erdw.ethz.ch).